Λ_b polarization in Z^0 decays at LEP

P. Abreu, W. Adam, T. Adye, P. Adzic, I. Azhinenko, Z. Albrecht, T. Alderweireld, G.D. Alekseev, R. Alemany, T. Allmendinger, et al.

Λ_b Polarization in Z^0 decays at LEP

DELPHI Collaboration

Abstract

The longitudinal polarization of the Λ_b baryon is measured at the LEP e^+e^- collider by DELPHI. It is determined from the charged lepton and neutrino energy spectra in 249±19 Λ_b semileptonic decays reconstructed in $\approx$3.5 million hadronic Z^0 decays using Λ^0-lepton correlations. The measured polarization is:

$$P_{\Lambda_b} = -0.49 \, ^{+0.32}_{-0.30}(stat.) \, \pm 0.17(syst.)$$

P.Abreu[22], W.Adam[52], T.Adye[38], P.Adzic[12], I.Ajinenko[44], Z.Albrecht[18], T.Alderweireld[2], G.D.Alekseev[17], R.Alemany[51], T.Allmendinger[18], P.P.Allport[23], S.Almehed[25], U.Amaldi[9], N.Amapane[47], S.Amato[49], E.G.Anassontzis[3], P.Andersson[46], A.Andreazza[9], S.Andringa[22], P.Antilogus[26], W-D.Apel[18], Y.Arnoud[9], B.Åsman[46], J-E.Augustin[26], A.Augustinus[9], P.Baillon[9], P.Bambade[20], F.Barao[22], G.Barbiellini[48], R.Barbier[26], D.Y.Bardin[17], G.Barker[18], A.Baroncelli[40], M.Battaglia[16], M.Baubillier[24], K-H.Becks[54], M.Begalli[6], A.Behrmann[54], P.Beilliere[8], Yu.Belokopytov[9], N.C.Benekos[33], A.C.Benvenuti[5], C.Berat[15], M.Berggren[26], D.Bertini[26], D.Bertrand[2], M.Besancon[41], M.Bigi[47], M.S.Bilenky[17], M-A.Bizouard[20], D.Bloch[10], H.M.Blom[32], M.Bonesini[29], W.Bonivento[28], M.Boonekamp[41], P.S.L.Booth[23], A.W.Borgland[4], G.Borisov[20], C.Bosio[43], O.Botner[50], E.Boudinov[32], B.Bouquet[20], C.Bourdarios[20], T.J.V.Bowcock[23], I.Boyko[17], I.Bozovic[12], M.Bozzo[14], M.Bracko[45], P.Branchini[40], R.A.Brenner[50], P.Bruckman[9], J-M.Brunet[8], L.Bugge[34], T.Buran[34], B.Buschbeck[52], P.Buschmann[54], S.Cabrera[51], M.Caccia[28], M.Calvi[29], T.Camporesi[9], V.Canale[39], F.Carena[9], L.Carroll[23], C.Caso[14], M.V.Castillo Gimenez[51], A.Cattai[9], F.R.Cavallo[5], V.Chabaud[9], Ph.Charpentier[9], L.Chaussard[26], P.Checchia[37], G.A.Chelkov[17], R.Chierici[47], P.Chliapnikov[9,44], P.Chochula[7], V.Chorowicz[26], J.Chudoba[31], K.Cieslik[19], P.Collins[9], R.Contri[14], E.Cortina[51], G.Cosme[20], F.Cossutti[9], H.B.Crawley[1], D.Crennell[38], S.Crepe[15], G.Crosetti[14], J.Cuevas Maestro[35], S.Czellar[16], M.Davenport[9], W.Da Silva[24], G.Della Ricca[48], P.Delpierre[27], N.Demaria[9], A.De Angelis[48], W.De Boer[18], C.De Clercq[2], B.De Lotto[48], A.De Min[37], L.De Paula[49], H.Dijkstra[9], L.Di Ciaccio[9,39], J.Dolbeau[8], K.Doroba[53], M.Dracos[10], J.Drees[54], M.Dris[33], A.Duperrin[26], J-D.Durand[9], G.Eigen[4], T.Ekelof[50], G.Ekspong[46], M.Ellert[50], M.Elsing[9], J-P.Engel[10], M.Espirito Santo[22], G.Fanourakis[12], D.Fassouliotis[12], J.Fayot[24], M.Feindt[18], A.Fenyuk[44], P.Ferrari[28], A.Ferrer[51], E.Ferrer-Ribas[20], F.Ferro[14], S.Fichet[24], A.Firestone[1], U.Flagmeyer[54], H.Foeth[9], E.Fokitis[33], F.Fontanelli[14], B.Franek[38], A.G.Frodesen[4], R.Fruhwirth[52], F.Fulda-Quenzer[20], J.Fuster[51], A.Galloni[23], D.Gamba[47], S.Gamblin[20], M.Gandelman[49], C.Garcia[51], C.Gaspar[9], M.Gaspar[49], U.Gasparini[37], Ph.Gavillet[9], E.N.Gazis[33], D.Gele[10], N.Ghodbane[26], I.Gil[51], F.Glege[54], R.Gokieli[9,53], B.Golob[9,45], G.Gomez-Ceballos[42], P.Goncalves[22], I.Gonzalez Caballero[42], G.Gopal[38], L.Gorn[1], Yu.Gouz[44], V.Gracco[14], J.Grahl[1], E.Graziani[40], P.Gris[41], G.Grosdidier[20], K.Grzelak[53], J.Guy[38], F.Hahn[9], S.Hahn[54], S.Haider[9], A.Hallgren[50], K.Hamacher[54], J.Hansen[34], F.J.Harris[36], V.Hedberg[9,25], S.Heising[18], J.J.Hernandez[51], P.Herquet[2], H.Herr[9], T.L.Hessing[36], J.-M.Heuser[54], E.Higon[51], S-O.Holmgren[46], P.J.Holt[36], S.Hoorelbeke[2], M.Houlden[23], J.Hrubec[52], M.Huber[18], K.Huet[2], G.J.Hughes[23], K.Hultqvist[9,46], J.N.Jackson[23], R.Jacobsson[9], P.Jalocha[19], R.Janik[7], Ch.Jarlskog[25], G.Jarlskog[25], P.Jarry[41], B.Jean-Marie[20], D.Jeans[36], E.K.Johansson[46], P.Jonsson[26], C.Joram[9], P.Juillot[10], L.Jungermann[18], F.Kapusta[24], K.Karafasoulis[12], S.Katsanevas[26], E.C.Katsoufis[33], R.Keranen[18], G.Kernel[45], B.P.Kersevan[45], B.A.Khomenko[17], N.N.Khovanski[17], A.Kiiskinen[16], B.King[23], A.Kinvig[23], N.J.Kjaer[9], O.Klapp[54], H.Klein[9], P.Kluit[32], P.Kokkinias[12], V.Kostioukhine[44], C.Kourkoumelis[3], O.Kouznetsov[41], M.Krammer[52], E.Kriznic[45], Z.Krumstein[17], P.Kubinec[7], J.Kurowska[53], K.Kurvinen[16], J.W.Lamsa[1], D.W.Lane[1], V.Lapin[44], J-P.Laugier[41], R.Lauhakangas[16], G.Leder[52], F.Ledroit[15], V.Lefebure[2], L.Leinonen[46], A.Leisos[12], R.Leitner[31], G.Lenzen[54], V.Lepeltier[20], T.Lesiak[19], M.Lethuillier[41], J.Libby[36], W.Liebig[54], D.Liko[9], A.Lipniacka[9,46], I.Lippi[37], B.Loerstad[25], J.G.Loken[36], J.H.Lopes[49], J.M.Lopez[42], R.Lopez-Fernandez[15], D.Loukas[12], P.Lutz[41], L.Lyons[36], J.MacNaughton[52], J.R.Mahon[6], A.Maio[22], A.Malek[54], T.G.M.Malmgren[46], S.Maltezos[33], V.Malychev[17], F.Mandl[52], J.Marco[42], R.Marco[42], B.Marechal[49], M.Margoni[37], J-C.Marin[9], C.Mariotti[9], A.Markou[12], C.Martinez-Rivero[20], F.Martinez-Vidal[51], S.Marti i Garcia[9], J.Masik[13], N.Mastroyiannopoulos[12], F.Matorras[42], C.Matteuzzi[29], G.Matthiae[39], F.Mazzucato[37], M.Mazzucato[37], M.Mc Cubbin[23], R.Mc Kay[1], R.Mc Nulty[23], G.Mc Pherson[23], C.Meroni[28], W.T.Meyer[1], A.Miagkov[44], E.Migliore[9], L.Mirabito[26], W.A.Mitaroff[52], U.Mjoernmark[25], T.Moa[46], M.Moch[18], R.Moeller[30], K.Moenig[9,11], M.R.Monge[14], X.Moreau[24], P.Morettini[14], G.Morton[36], U.Mueller[54], K.Muenich[54], M.Mulders[32], C.Mulet-Marquis[15], R.Muresan[25], W.J.Murray[38], B.Muryn[19], G.Myatt[36], T.Myklebust[34], F.Naraghi[15], M.Nassiakou[12], F.L.Navarria[5], S.Navas[51], K.Nawrocki[53], P.Negri[29], N.Neufeld[9], R.Nicolaidou[41], B.S.Nielsen[30], P.Niezurawski[53], M.Nikolenko[10,17], V.Nomokonov[16], A.Nygren[25], V.Obraztsov[44], A.G.Olshevski[17], A.Onofre[22], R.Orava[16], G.Orazi[10], K.Osterberg[16], A.Ouraou[41], M.Paganoni[29], S.Paiano[5], R.Pain[24], R.Paiva[22], J.Palacios[36], H.Palka[19], Th.D.Papadopoulou[9,33], K.Papageorgiou[12], L.Pape[9], C.Parkes[9], F.Parodi[14], U.Parzefall[23], A.Passeri[40], O.Passon[54], T.Pavel[25], M.Pegoraro[37], L.Peralta[22], M.Pernicka[52], A.Perrotta[5], C.Petridou[48], A.Petrolini[14], H.T.Phillips[38], F.Pierre[41], M.Pimenta[22], E.Piotto[28], T.Podobnik[45], M.E.Pol[6], G.Polok[19], P.Poropat[48], V.Pozdniakov[17], P.Privitera[39], N.Pukhaeva[17], A.Pullia[29], D.Radojicic[36], S.Ragazzi[29], H.Rahmani[33], J.Rames[13], P.N.Ratoff[21], A.L.Read[34], P.Rebecchi[9], N.G.Redaelli[28], M.Regler[52], J.Rehn[18], D.Reid[32], R.Reinhardt[54], P.B.Renton[36], L.K.Resvanis[3], F.Richard[20], J.Ridky[13], G.Rinaudo[47], I.Ripp-Baudot[10], O.Rohne[34], A.Romero[47], P.Ronchese[37], E.I.Rosenberg[1], P.Rosinsky[7], P.Roudeau[20], T.Rovelli[5], Ch.Royon[41], V.Ruhlmann-Kleider[41], A.Ruiz[42], H.Saarikko[16], Y.Sacquin[41], A.Sadovsky[17], G.Sajot[15], J.Salt[51], D.Sampsonidis[12], M.Sannino[14], Ph.Schwemling[24], B.Schwering[54], U.Schwickerath[18], F.Scuri[48], P.Seager[21], Y.Sedykh[17], A.M.Segar[36], N.Seibert[18], R.Sekulin[38], R.C.Shellard[6], M.Siebel[54], L.Simard[41], F.Simonetto[37], A.N.Sisakian[17], G.Smadja[26], N.Smirnov[44], O.Smirnova[25], G.R.Smith[38], A.Sopczak[18], R.Sosnowski[53], T.Spassov[22], E.Spiriti[40], S.Squarcia[14], C.Stanescu[40], S.Stanic[45], M.Stanitzki[18], K.Stevenson[36], A.Stocchi[20], J.Strauss[52], R.Strub[10], B.Stugu[4], M.Szczekowski[53], M.Szeptycka[53], T.Tabarelli[29], A.Taffard[23], O.Tchikilev[44], F.Tegenfeldt[50], F.Terranova[29], J.Thomas[36], J.Timmermans[32], N.Tinti[5], L.G.Tkatchev[17], M.Tobin[23], S.Todorova[10], A.Tomaradze[2], B.Tome[22], A.Tonazzo[9], L.Tortora[40], P.Tortosa[51], G.Transtromer[25], D.Treille[9],

G.Tristram[8], M.Trochimczuk[53], C.Troncon[28], M-L.Turluer[41], I.A.Tyapkin[17], S.Tzamarias[12], O.Ullaland[9], V.Uvarov[44], G.Valenti[9,5], E.Vallazza[48], P.Van Dam[32], W.Van den Boeck[2], J.Van Eldik[9,32], A.Van Lysebetten[2], N.van Remortel[2], I.Van Vulpen[32], G.Vegni[28], L.Ventura[37], W.Venus[38,9], F.Verbeure[2], M.Verlato[37], L.S.Vertogradov[17], V.Verzi[39], D.Vilanova[41], L.Vitale[48], E.Vlasov[44], A.S.Vodopyanov[17], G.Voulgaris[3], V.Vrba[13], H.Wahlen[54], C.Walck[46], A.J.Washbrook[23], C.Weiser[9], D.Wicke[54], J.H.Wickens[2], G.R.Wilkinson[36], M.Winter[10], M.Witek[19], G.Wolf[9], J.Yi[1], O.Yushchenko[44], A.Zalewska[19], P.Zalewski[53], D.Zavrtanik[45], E.Zevgolatakos[12], N.I.Zimin[17,25], A.Zintchenko[17], Ph.Zoller[10], G.C.Zucchelli[46], G.Zumerle[37]

[1] Department of Physics and Astronomy, Iowa State University, Ames IA 50011-3160, USA
[2] Physics Department, Univ. Instelling Antwerpen, Universiteitsplein 1, B-2610 Antwerpen, Belgium
  and IIHE, ULB-VUB, Pleinlaan 2, B-1050 Brussels, Belgium
  and Faculté des Sciences, Univ. de l'Etat Mons, Av. Maistriau 19, B-7000 Mons, Belgium
[3] Physics Laboratory, University of Athens, Solonos Str. 104, GR-10680 Athens, Greece
[4] Department of Physics, University of Bergen, Allégaten 55, NO-5007 Bergen, Norway
[5] Dipartimento di Fisica, Università di Bologna and INFN, Via Irnerio 46, IT-40126 Bologna, Italy
[6] Centro Brasileiro de Pesquisas Físicas, rua Xavier Sigaud 150, BR-22290 Rio de Janeiro, Brazil
  and Depto. de Física, Pont. Univ. Católica, C.P. 38071 BR-22453 Rio de Janeiro, Brazil
  and Inst. de Física, Univ. Estadual do Rio de Janeiro, rua São Francisco Xavier 524, Rio de Janeiro, Brazil
[7] Comenius University, Faculty of Mathematics and Physics, Mlynska Dolina, SK-84215 Bratislava, Slovakia
[8] Collège de France, Lab. de Physique Corpusculaire, IN2P3-CNRS, FR-75231 Paris Cedex 05, France
[9] CERN, CH-1211 Geneva 23, Switzerland
[10] Institut de Recherches Subatomiques, IN2P3 - CNRS/ULP - BP20, FR-67037 Strasbourg Cedex, France
[11] Now at DESY-Zeuthen, Platanenallee 6, D-15735 Zeuthen, Germany
[12] Institute of Nuclear Physics, N.C.S.R. Demokritos, P.O. Box 60228, GR-15310 Athens, Greece
[13] FZU, Inst. of Phys. of the C.A.S. High Energy Physics Division, Na Slovance 2, CZ-180 40, Praha 8, Czech Republic
[14] Dipartimento di Fisica, Università di Genova and INFN, Via Dodecaneso 33, IT-16146 Genova, Italy
[15] Institut des Sciences Nucléaires, IN2P3-CNRS, Université de Grenoble 1, FR-38026 Grenoble Cedex, France
[16] Helsinki Institute of Physics, HIP, P.O. Box 9, FI-00014 Helsinki, Finland
[17] Joint Institute for Nuclear Research, Dubna, Head Post Office, P.O. Box 79, RU-101 000 Moscow, Russian Federation
[18] Institut für Experimentelle Kernphysik, Universität Karlsruhe, Postfach 6980, DE-76128 Karlsruhe, Germany
[19] Institute of Nuclear Physics and University of Mining and Metalurgy, Ul. Kawiory 26a, PL-30055 Krakow, Poland
[20] Université de Paris-Sud, Lab. de l'Accélérateur Linéaire, IN2P3-CNRS, Bât. 200, FR-91405 Orsay Cedex, France
[21] School of Physics and Chemistry, University of Lancaster, Lancaster LA1 4YB, UK
[22] LIP, IST, FCUL - Av. Elias Garcia, 14-1°, PT-1000 Lisboa Codex, Portugal
[23] Department of Physics, University of Liverpool, P.O. Box 147, Liverpool L69 3BX, UK
[24] LPNHE, IN2P3-CNRS, Univ. Paris VI et VII, Tour 33 (RdC), 4 place Jussieu, FR-75252 Paris Cedex 05, France
[25] Department of Physics, University of Lund, Sölvegatan 14, SE-223 63 Lund, Sweden
[26] Université Claude Bernard de Lyon, IPNL, IN2P3-CNRS, FR-69622 Villeurbanne Cedex, France
[27] Univ. d'Aix - Marseille II - CPP, IN2P3-CNRS, FR-13288 Marseille Cedex 09, France
[28] Dipartimento di Fisica, Università di Milano and INFN, Via Celoria 16, IT-20133 Milan, Italy
[29] Università degli Studi di Milano - Bicocca, Via Emanuelli 15, IT-20126 Milan, Italy
[30] Niels Bohr Institute, Blegdamsvej 17, DK-2100 Copenhagen Ø, Denmark
[31] IPNP of MFF, Charles Univ., Areal MFF, V Holesovickach 2, CZ-180 00, Praha 8, Czech Republic
[32] NIKHEF, Postbus 41882, NL-1009 DB Amsterdam, The Netherlands
[33] National Technical University, Physics Department, Zografou Campus, GR-15773 Athens, Greece
[34] Physics Department, University of Oslo, Blindern, NO-1000 Oslo 3, Norway
[35] Dpto. Fisica, Univ. Oviedo, Avda. Calvo Sotelo s/n, ES-33007 Oviedo, Spain
[36] Department of Physics, University of Oxford, Keble Road, Oxford OX1 3RH, UK
[37] Dipartimento di Fisica, Università di Padova and INFN, Via Marzolo 8, IT-35131 Padua, Italy
[38] Rutherford Appleton Laboratory, Chilton, Didcot OX11 OQX, UK
[39] Dipartimento di Fisica, Università di Roma II and INFN, Tor Vergata, IT-00173 Rome, Italy
[40] Dipartimento di Fisica, Università di Roma III and INFN, Via della Vasca Navale 84, IT-00146 Rome, Italy
[41] DAPNIA/Service de Physique des Particules, CEA-Saclay, FR-91191 Gif-sur-Yvette Cedex, France
[42] Instituto de Fisica de Cantabria (CSIC-UC), Avda. los Castros s/n, ES-39006 Santander, Spain
[43] Dipartimento di Fisica, Università degli Studi di Roma La Sapienza, Piazzale Aldo Moro 2, IT-00185 Rome, Italy
[44] Inst. for High Energy Physics, Serpukov P.O. Box 35, Protvino, (Moscow Region), Russian Federation
[45] J. Stefan Institute, Jamova 39, SI-1000 Ljubljana, Slovenia and Laboratory for Astroparticle Physics,
  Nova Gorica Polytechnic, Kostanjeviska 16a, SI-5000 Nova Gorica, Slovenia,
  and Department of Physics, University of Ljubljana, SI-1000 Ljubljana, Slovenia
[46] Fysikum, Stockholm University, Box 6730, SE-113 85 Stockholm, Sweden
[47] Dipartimento di Fisica Sperimentale, Università di Torino and INFN, Via P. Giuria 1, IT-10125 Turin, Italy
[48] Dipartimento di Fisica, Università di Trieste and INFN, Via A. Valerio 2, IT-34127 Trieste, Italy
  and Istituto di Fisica, Università di Udine, IT-33100 Udine, Italy
[49] Univ. Federal do Rio de Janeiro, C.P. 68528 Cidade Univ., Ilha do Fundão BR-21945-970 Rio de Janeiro, Brazil
[50] Department of Radiation Sciences, University of Uppsala, P.O. Box 535, SE-751 21 Uppsala, Sweden
[51] IFIC, Valencia-CSIC, and D.F.A.M.N., U. de Valencia, Avda. Dr. Moliner 50, ES-46100 Burjassot (Valencia), Spain
[52] Institut für Hochenergiephysik, Österr. Akad. d. Wissensch., Nikolsdorfergasse 18, AT-1050 Vienna, Austria
[53] Inst. Nuclear Studies and University of Warsaw, Ul. Hoza 69, PL-00681 Warsaw, Poland
[54] Fachbereich Physik, University of Wuppertal, Postfach 100 127, DE-42097 Wuppertal, Germany

1 Introduction

A measurement of the Λ_b baryon polarization at the LEP e^+e^- collider is presented using the hadronic Z^0 decays collected by DELPHI in the years 1992–1995. Semileptonic Λ_b decays are reconstructed inclusively looking for the $\Lambda^0 l\nu X$ final states.

A large longitudinal polarization of the Λ_b is a direct consequence of the polarization of primary b quark coming from a Z^0 decay. The polarization of fermions produced in the reaction $e^+e^- \to Z^0 \to f\bar{f}$ is precisely predicted in the framework of the SM (**S**tandard **M**odel). In the case of unpolarized e^+e^- beams the average longitudinal polarization of a b quark is predicted to be [1,2]:

$$\langle P_b \rangle \simeq -0.94 \tag{1}$$

Neither gluon nor photon radiation from the final state are predicted to degrade this high polarization significantly. One-loop QCD mass effects reduce it by an amount of 3% only [3,4]. The first possibility of altering the primary b quark spin state arises during (and after) hadronization.

In the Heavy Quark Effective Theory approximation (HQET) [5] the spin degrees of freedom of a heavy quark are decoupled from a spin-zero light diquark. Therefore in the heavy quark limit a b quark hadronizing directly to a Λ_b should pass its complete initial polarization to the baryon and then conserve it throughout the whole Λ_b lifetime.

However, b quark fragmentation into Σ_b and Σ_b^* states which subsequently decay strongly into a $\Lambda_b + \pi$ can lead to a substantial depolarization of the heavy quark if the two $\Sigma_b^{(*)}$ states live long enough to form distinct narrow resonances. A detailed discussion of different scenarios of the indirect hadronization is given in [6,7]. Figure 1 shows the prediction for the effective Λ_b polarization as a function of the fraction of Λ_b's produced indirectly through Σ_b and Σ_b^* states (f_{Σ_b}). The prediction takes into account all possible spin alignments of the light diquark in hadronization into $\Sigma_b^{(*)}$. Two boundaries $w_1 = 0$ and $w_1 = 2/3$ correspond to the spin alignment suppression (strongest depolarization) and isotropic spin distribution respectively. Yet, there is no strong experimental evidence for the $\Sigma_b^{(*)}$ production. However, motivated by the measurements in the *strange* sector we expect them to be produced copiously [8,9]. The JETSET [10] event generator default parameters lead to about 30% of Λ_b's being produced indirectly in the decays of $\Sigma_b^{(*)}$ baryons. This corresponds to the effective Λ_b polarization in the range $-0.67 \geq P_{effective} \geq -0.75$.

In the Born approximation of the free quark semileptonic decay $b \to c + l + \bar{\nu}$ the matrix element exhibits a factorisation of the spin direction component [11,12]:

$$|\mathcal{M}|^2 \cong |\mathcal{M}_{unpol}|^2 (1 + P cos\theta) \tag{2}$$

where P denotes the b polarization and θ is the angle between the neutrino three-momentum and the spin quantization axis in the b rest frame. $|\mathcal{M}_{unpol}|^2$ is the decay matrix element of the unpolarized b. QCD correction terms violate the factorisation (2) only at the percent level [11–13]. Being very small compared to the present experimental accuracy they were considered negligible. It can be also argued that when going to real heavy baryon decays, the dynamics of the reaction $\Lambda_b \to \Lambda_c^+ l^- \nu$ remains identical with the free quark case discussed above [14]. This approximation is derived from the leading order of the HQET and the remaining mass corrections are negligibly small [15,16].

The $\bar{b}$ quarks are produced with polarization opposite to that of the b quarks ($\bar{b}$ has positive polarization). However from the CP invariance of the weak decay $\Lambda_b \to \Lambda_c^+ l^- \nu$ the final differential distributions of the charged lepton and neutrino look the same after

the charge conjugation operation. Consequently, both Λ_b and $\bar{\Lambda}_b$ semileptonic decays lead to the same momentum distributions of the decay products. Hereafter, the antiparticles are always implied.

The paper is organised as follows. The experimental method is explained in section 2. Section 3 briefly describes the DELPHI spectrometer. Section 4 contains a description of the analysis procedure: the Λ_b signal selection (4.1,4.2,4.3), the possible background sources (4.4) and the reconstruction of the neutrino energy which carries most sensitivity to the Λ_b polarization (4.5). The results of the measurement and a discussion of the systematic uncertainties are presented in section 5. This section also presents the result of the analogous polarization measurement performed on B mesons, serving as a consistency check of the analysis. The conclusions are given in section 6.

2   Principles of the measurement

Λ_b polarization is studied in its semileptonic decays with a Λ^0 reconstructed in the final state. These decays have the following properties: the lepton is highly energetic and has high transverse momentum relative to the jet axis and the Λ^0 has a harder momentum spectrum than the Λ^0 baryons produced from fragmentation. Moreover, $\Lambda^0 l$ pairs originating from a b baryon cascade have a well defined correlation between the lepton charge and the Λ^0 baryonic number. For brevity it will be called charge correlation. The b baryon signal is uniquely related to $\Lambda^0 l^-$ (or $\bar{\Lambda}^0 l^+$) correlations, hereafter called *right-sign* (R.S.). $\Lambda^0 l^+$ (or $\bar{\Lambda}^0 l^-$) correlations, hereafter called *wrong-sign* (W.S.), have a purely background origin. As will be shown in section 4.4, the great majority of background events have no physically preferred charge correlation and therefore are equally distributed among the two classes. Hence, the excess of *right-sign* events over *wrong-sign* ones is attributed to the semileptonic decays of the Λ_b baryon.

Neither the Λ_b four-momentum nor the neutrino four-momentum can be fully reconstructed in the experiment. However, Λ_b baryons produced at LEP are highly boosted in the laboratory frame. In such a case the forward-backward asymmetry of a decay product can be directly expressed in terms of a shift in the average value of its energy. The charged lepton also carries a residual sensitivity to the Λ_b polarization. It is not explicit in formula (2) but arises as a reflection of the neutrino dependence from the four-momentum conservation. It follows that the average energies of the charged lepton, $\langle E_l \rangle$, and the neutrino, $\langle E_\nu \rangle$, are respectively anti-correlated and correlated with the polarization. Hence, the quantity defined as:

$$y = \frac{\langle E_l \rangle}{\langle E_\nu \rangle} \tag{3}$$

is highly sensitive to Λ_b polarization and is explicitly independent of fragmentation uncertainties [17].

In reality the observed energy spectra undergo several deformations because of detector response and selection cuts. To correct for these effects the variable y obtained from the data was normalised to the one extracted from a sample of unpolarized simulated events. Therefore, the final variable is defined:

$$R_y = \frac{y^{DATA}}{y^{MC}_{P=0}}. \tag{4}$$

Plots in Fig. 2 show the actual experimental response of polarization observables to the Λ_b polarization after the entire reconstruction as obtained from the background-free

simulation described in section 4. Plots (a) and (b) were fitted with linear functions, as expected from the theory. Because of the constraint ($f(0) = 1$) there was only one free parameter in each fit. The curve in Fig. 2c representing the ratio of (a) and (b) resulted from a fit to the $y/y_{P=0}$ points with the function $f(x) = \frac{P_1 - x}{P_1 + P_2 x}$. This calibration curve will be used to extract the polarization of Λ_b after determining the value of R_y from data.

Other polarization observables proposed in [18] ($y_2 = \frac{\langle E_l^2 \rangle}{\langle E_\nu^2 \rangle}$ and $y_3 = \left\langle \frac{E_\nu}{E_l} \right\rangle$) were also investigated. No improvement in the sensitivity to polarization was observed. None of these discriminating variables is a priori guaranteed to be well reproduced in the simulation and hence they can be a potential source of systematic uncertainty. Only systematics related to the chosen y variable were studied in detail. In addition to all systematic uncertainties present already in y, the y_2 variable exhibits dependence on the energy spectra widths and y_3 is sensitive to event-by-event lepton neutrino correlations.

All proposed approaches require a good knowledge of the escaping neutrino energy E_ν. In the LEP environment such a determination is achievable using the hemisphere missing energy method described in detail in section 4.5.

Polarization of the Λ^0 from the cascade although experimentally accessible does not have a direct simple connection to the Λ_b polarization. Correlation between the two polarizations depends strongly on the Λ_c decay channel as well as on the possible existence of heavier baryonic resonances in the decay cascade. Therefore, information coming from the Λ^0 polarization was not used in this measurement.

3   The DELPHI spectrometer

A complete description of the DELPHI spectrometer and its performance can be found in [19] and [20]. In this section only the characteristics most relevant for this analysis are summarised.

The detector elements used for tracking were the Vertex Detector (VD), the Inner Detector (ID), the Time Projection Chamber (TPC) and the Outer Detector (OD). In this central region, a highly uniform magnetic field of 1.23 T parallel to the $e^+ e^-$ beam direction was provided by the superconducting solenoid. Charged particle tracks were reconstructed with a precision $\sigma_p / p < 2.0 \times 10^{-3} p$ (p in GeV/c) in the polar angle region $25° < \theta < 155°$. In the forward region there were two additional tracking devices: Forward Chambers A (FCA) and Forward Chambers B (FCB). The sensitive area of these drift chambers covered polar angles $11° \leq \theta \leq 36°$ and $144° \leq \theta \leq 169°$.

Calorimeters detected photons and neutral hadrons by the total absorption of their energy. Electromagnetic calorimeters served also as the main devices for electron identification (see section 4.1). The electromagnetic calorimetry system of DELPHI was composed of a barrel calorimeter, the HPC, covering the polar angle region $46° < \theta < 134°$, and forward calorimeters, the FEMC, for polar angles $8° < \theta < 35°$ and $145° < \theta < 172°$. The relative precision on the measured energy E was parametrised as $\sigma_E / E = 0.32/\sqrt{E} \oplus 0.043$ (E in GeV) in the barrel, and $\sigma_E / E = 0.12/\sqrt{E} \oplus 0.03$ (E in GeV) in the forward region. The hadron calorimeter, HCAL, was installed in the return yoke of the DELPHI solenoid. In the barrel region, the energy was reconstructed with a precision of $\sigma_E / E = 1.12/\sqrt{E} \oplus 0.21$ (E in GeV).

Muon identification was provided by the muon chambers. In the barrel region they consisted of three layers covering the polar angle regions $53° < \theta < 88.5°$ and $91.5° < \theta < 127°$. The first layer contained three planes of chambers and was inside the return yoke of the magnet after 90 cm of iron, while the other two, with two chamber

planes each, were mounted outside the yoke behind a further 20 cm of iron. In the end-caps there were two layers of muon chambers mounted one outside and one just inside the return yoke of the magnet. Each consisted of two planes of active chambers covering the polar angle regions $20° < \theta < 42°$ and $138° < \theta < 160°$ where the charged particle tracking was efficient.

4   Analysis procedure

The analysis was based on 3.5×10^6 hadronic Z^0 decays collected by the DELPHI detector in the 1992 to 1995 data-taking periods. A large sample of background-free $b \to \Lambda_b$ simulated events was used to determine the calibration curve of Fig. 2c and to evaluate the reference value y^{MC} of the quantity y (see formulae (3) and (4)). From this sample over 2,000 candidates for the cascade decay $\Lambda_b \to l\nu\Lambda^0 X$ remain after the whole reconstruction and the complete analysis selection. To cross-check the signal selection and result extraction, a sample of 5.5×10^6 simulated hadronic Z^0 events (unbiased $q\bar{q}$) was used. In both cases events were generated using the JETSET [10] generator with parton shower option and the DELPHI tuning [21]. The Λ_b semileptonic decays were generated explicitly unpolarized and without QCD corrections, i.e. according to: $|\mathcal{M}|^2 = (\boldsymbol{cl})(\boldsymbol{b\nu})$. The Λ_b polarization in the background-free signal sample was then simulated by reweighting events according to the approximation of equation (2).

4.1   Lepton identification

Lepton identification in the DELPHI detector was based on the electromagnetic calorimeters (for electrons) and the muon chambers (for muons). Therefore, the angular coverage of the identification was limited by the acceptance of the above devices (see section 3). Only particles with momentum larger than 3 GeV/c were considered as possible lepton candidates.

The χ^2 of the match between the track extrapolation to the muon chambers and the observed hits gave the probability of the lepton candidate being a muon. With the selections applied, inside the angular acceptance of the muon chambers the muon identification efficiency was $(95 \pm 1)\%$ and the hadron misidentification probability $(1.5 \pm 0.1)\%$.

The probability of a lepton candidate being an electron was calculated using a comparison between its momentum reconstructed in the tracking devices and the energy of associated electromagnetic shower reconstructed in the HPC or FEMC. In the HPC a fit to the longitudinal profile of the electromagnetic shower was performed as well. An independent dE/dX measurement in the TPC leads to additional $e - \pi$ separation. With the selections and inside the angular acceptance of the HPC and FEMC, the electron identification efficiency was found to be $(55 \pm 1)\%$ and the hadron misidentification probability 0.4%.

Lepton candidates selected using the identification tools described above had to satisfy further quality requirements: track length > 30 cm, relative error on momentum $< 25\%$, impact parameter to the interaction point < 4 cm in the plane transverse to the beam and < 10 cm in the beam direction. In addition, electron candidates were rejected in cases where they matched the photon conversion hypothesis tagged by a successful vertex fit with an oppositely charged electron candidate giving an invariant mass below 20 MeV/c^2.

4.2 Λ^0 reconstruction

Λ^0 candidates were reconstructed in the channel $\Lambda^0 \to p\pi^-$. The reconstruction of the V^0 vertex and selection cuts are described in detail in reference [20]. The $\Lambda^0 \to p\pi^-$ reconstruction efficiency depended strongly on the Λ^0 momentum, and varied between 35% and 10%.

In the analysis presented here only Λ^0 candidates with $p_\Lambda > 5$ GeV/c were selected. This requirement suppresses the large background due to low energy Λ^0's from fragmentation. To extract the signal of the Λ_b baryons, Λ^0 candidates with an invariant mass of the pπ^- system within two standard deviations from the nominal Λ^0 mass were used. The Λ^0 decay product with the higher momentum was assumed to be the proton. Its charge determined the Λ^0 baryon number.

4.3 Λ_b signal selection

All events had to satisfy the selection criteria defining hadronic events from Z^0 decays, requiring a charged multiplicity greater than four and a total energy of charged particles greater than $0.12\sqrt{s}$, where $\sqrt{s}$ was the centre-of-mass energy and all particles were assumed to be pions; charged particles were required to have a momentum greater than 0.4 GeV/c and a polar angle between 20° and 160°. The overall trigger and selection efficiency was over 95%. The background, mainly from $\tau^+\tau^-$ pairs with a smaller contribution from $\gamma\gamma$ collisions, was below 0.7% [20]. Additionally, events were dropped when the central tracking detectors (in particular TPC) and both electromagnetic and hadronic calorimeters were not fully operational. In total 3,498,225 events were selected for analysis.

Events were subdivided into two hemispheres by a plane perpendicular to the thrust axis and containing the interaction point. Each event was required to have the thrust axis more than 30° from the beam directions since for the missing energy measurement it was essential to have events well contained in the detector fiducial volume where the reconstruction efficiency is high and well controlled. In order to suppress events with hard gluon radiation the calculated thrust value was required to exceed 0.75. The total visible energy in an event had to be between 30 GeV and 130 GeV.

Events with the combination of a charged lepton and a Λ^0 in the same hemisphere were searched for. The initial sample of $\Lambda^0 l$ pairs still contained a large fraction of background events mainly due to Λ^0 baryons from fragmentation and from non-b events. To reduce this background the following kinematic selections were applied:

- The transverse momentum of the lepton to the nearest particle jet, p_T, was required to be greater than 0.8 GeV/c. The LUCLUS jet finding algorithm [10] was used with $d_{join} = 2.5$ GeV and excluding the lepton from the jet.
- The invariant mass of the Λ and the lepton had to lie in the range 2.1 to 4.5 GeV/c^2.
- The momentum of the Λl system had to exceed 11.0 GeV/c.
- The angle between the lepton momentum direction and the Λ momentum direction could not be larger than 90°.
- The angle between the momentum of the Λl system and the thrust direction was required to be smaller than 45°.

The first selection enriches the sample in leptons from semileptonic b decays. The next two cuts suppress contribution from Λ_c semileptonic decays and accidental combinations. The last two selections are fairly loose and mainly guard against accidental combinations where either the lepton or the Λ^0 belongs to a distinct hard gluon jet.

An algorithm to tag b quark decays was also applied. This is based on the long b hadron lifetimes and uses the large track impact parameters of the decay products [20]. The output from the b tagging algorithm is expressed in terms of the probability that all charged particle tracks originate from a common primary vertex. b events have their probabilities strongly peaked at zero while light quark ones have probabilities uniformly distributed from zero to one. The cut $P_{b-TAG} < 0.05$ was applied to the selected event sample. This cut suppresses $\approx 50\%$ of the background but only about 15% of the signal which corresponds to a drop of the background fraction from 56% to 41% . Most of the remaining background comes from B events.

The overall efficiency to reconstruct the decay $\Lambda_b^0 \to l^- \bar{\nu}_l \Lambda^0 X$ (where all decay modes for the Λ^0 were assumed) was found to be 0.030 ± 0.001 in the simulation. However, the actual knowledge of this efficiency is not needed for the polarization measurement. Only the signal purity was used and was measured using the data, as will be shown later.

The reconstructed Λ^0 mass distributions for *right-sign* and *wrong-sign* $\Lambda^0 l$ charge correlations observed in the data after the b-tagging cut are shown in Fig. 3. The excess of *right-sign* correlations over *wrong-sign* ones in the Λ^0 mass peak amounts to 249 ± 19 Λ_b candidates. The width of the Λ^0 mass acceptance window depends on the $(p\pi^-)$ momentum and grows linearly from ± 9 MeV/c^2 (at 5 GeV/c) to ± 38 MeV/c^2 (at 30 GeV/c).

4.4   Background estimation and subtraction

To extract the average charged lepton and neutrino energies for the Λ_b signal, both the background fraction and the corresponding charged lepton and neutrino average energies in the *right-sign* sample background have to be known. In the following it will be shown that the background contained in the *right-sign* sample is to a good approximation mimicked by the *wrong-sign* sample. The study uses the simulated hadronic Z^0 events described in section 4 on which the complete Λ_b signal selection was performed. The composition of the *right-sign* and the *wrong-sign* samples after normalizing to the luminosity of the real data is summarised in Table 1. The table also gives the total number of events in the two sign combinations reconstructed in the data. The Λ_b production rate is overestimated in the Monte Carlo. However, the amount of background is compatible in the two samples.

All events in which the true lepton from the Λ_b decay was reconstructed and identified were considered as the $\Lambda_b \to l\nu X$ signal. The great majority of these events contributed to the *right-sign* correlations. Candidates with opposite correlations originated from either fragmentation or fake Λ^0's.

All b-baryon hadronic decays where the lepton candidate was either misidentified or did not come from the b semileptonic decay were classified as b-baryon background. In this category the great majority of events contained a true Λ^0 from the baryon cascade. Here there are two physical sources of definite sign combinations. The first one, b-baryon $\to c$-baryon $\to l^+ \nu_l \Lambda^0 X$ where the lepton from the semileptonic c decay has been selected, is a source of *wrong-sign* combinations. It is highly suppressed by requiring a high lepton p_T and the mass of the $\Lambda^0 l$ system to exceed 2.1 GeV/c^2; its contribution to the total background is smaller than 2% . The second one, b-baryon $\to \tau \bar{\nu}_\tau \Lambda^0 X$ where $\tau \to \nu_\tau l \bar{\nu}_l$, is a source of *right-sign* combinations. The BR($b \to \tau^- \to l^-$) has been experimentally estimated to be $(0.7 \pm 0.2)\%$ [22] and is not negligible. Some attenuation of this signal is obtained by requiring a high momentum lepton (> 3.0 GeV) since the lepton from the τ cascade is less energetic. From the Monte Carlo estimation the τ

event category	Right-Sign	Wrong-Sign
$\Lambda_b \to l\nu X$ signal	421.9±16.4	25.5±4.0
b–baryon background	19.7±3.5	17.8±3.4
B mesons	134.0±9.2	122.8±8.8
c–jets	13.4±2.9	24±3.9
u, d, s or g	24.8±4.0	14.6±3.1
total background	192.2±11.1	179.5±10.7
total events in 1992–1995 data	422±21	173±13

Table 1: Composition of the *right-sign* and *wrong-sign* event samples from simulation after applying all selection criteria and normalizing to the luminosity of the real data. The total numbers in the real data are also shown.

background gives a small contribution (about 3%), but since it is characterised by exceptionally high missing energy (low y values) it can lead to a perceptible systematic shift. The high missing energy comes from the fact that there are three escaping neutrinos in the process.

Table 1 shows that the majority of the background comes from B mesons. Most of it is from accidental combinations which are not biased towards either sign combination. However, in the meson sample there are possible sources of biases between *right-sign* and *wrong-sign* samples. From a more extensive study using the JETSET [10] Monte Carlo event generator we find a systematic tendency towards 10% excess in the *right-sign* sample. Due to baryon number conservation, baryons are always produced in pairs in the fragmentation. The string fragmentation model used in the simulation has the effect that the more energetic baryon from fragmentation most likely contains the anti-partner of the light quark building the B meson. Therefore, requiring the Λ^0 momentum to be greater than 5.0 GeV/c favours pairs of the type: $(\bar{B} = b\bar{q}) + (qq'q'' = baryon)$ which contribute to the *right-sign* sample. The level of induced asymmetry depends on the details of the fragmentation and will be considered as a source of systematic uncertainty. Semileptonic B decays, such as $B \to \Lambda_c \bar{N} l \nu X$ (where $\bar{N}$ is an antibaryon) could also give rise to an excess of *right-sign* combinations. The actual branching fraction for such processes is yet not measured but from the available limits the contribution of this background has been estimated to be negligible [23].

Background originating from c quark jets apart from accidental combinations contains $\Lambda^0 l^+$ pairs from the process c-baryon $\to l^+ \Lambda^0 X$ which contribute to the *wrong-sign* sample. Their contribution is highly suppressed by cuts on the lepton p_T and mass of $\Lambda^0 l$ system and by the b-tagging. The contribution from this background is smaller than 2%.

Finally, the last class contains $\Lambda^0 l$ pairs reconstructed in the u, d, s or gluon jets. These combinations are purely accidental and hence are symmetrical in the sign combination.

Average energies of the charged lepton and the neutrino as well as the resulting y values in *right-sign* and *wrong-sign* background samples from simulation and in the *wrong-sign* data sample are given in Table 2. The values are in good agreement but possible biases arising from the particular physics processes discussed above will contribute to the systematic error.

	MC background Right-Sign (GeV)	MC background Wrong-Sign (GeV)	1992–1995 data Wrong-Sign (GeV)
$\langle E_l \rangle$	9.71±0.31	9.51±0.32	10.20±0.41
$\langle E_\nu \rangle$	5.08±0.38	5.23±0.39	5.61±0.50
y	$1.91^{+0.17}_{-0.14}$	$1.82^{+0.15}_{-0.14}$	$1.82^{+0.19}_{-0.17}$

Table 2: Average reconstructed charged lepton and neutrino energies and their ratio y in *right-sign* and *wrong-sign* simulation background and *wrong-sign* real data.

Since the *right-sign* background behaviour is well reproduced by the *wrong-sign* sample it is possible to extract the average charged lepton energy and the average neutrino energy originating from the Λ_b semileptonic decay using the following background subtraction:

$$\langle E_{l,\nu} \rangle = \frac{1}{1 - f_{bck}} (\langle E_{l,\nu}^{R.S.} \rangle - f_{bck} \langle E_{l,\nu}^{W.S.} \rangle) \quad and \quad f_{bck} = \frac{\mathrm{N}^{W.S.}}{\mathrm{N}^{R.S.}} \tag{5}$$

where $\langle E_{l,\nu}^{R.S.} \rangle$ and $\langle E_{l,\nu}^{W.S.} \rangle$ are the average charged lepton or neutrino energies measured in the *right-sign* and in the *wrong-sign* samples respectively. $\mathrm{N}^{R.S.}$ and $\mathrm{N}^{W.S.}$ are the number of selected events found in the *right-sign* and *wrong-sign* samples.

4.5   Neutrino energy reconstruction

The neutrino energy (E_ν) is not directly measurable in the experiment. It was approximated by the missing energy (E_{miss}) in the hemisphere containing the $\Lambda^0 l$ system (Λ_b hemisphere):

$$E_\nu \approx E_{miss} = E_{TOT} - E_{vis}$$
$$E_{TOT} = \frac{\sqrt{s}}{2} + \frac{(M^{\Lambda_b})^2 - (M^{oppo})^2}{2\sqrt{s}} \tag{6}$$

where E_{vis} is the sum of all charged particle energies and neutral calorimeter energy deposits in the Λ_b hemisphere. E_{TOT} is the total energy available in the Λ_b hemisphere. The lower equation results directly from four-momentum conservation applied to the entire event. M^{Λ_b} and M^{oppo} are the Λ_b hemisphere invariant mass and the opposite hemisphere invariant mass respectively. $\sqrt{s}$ denotes the total energy in the center-of-mass of the colliding $e^+ e^-$. Individual energy deposits in both electromagnetic calorimeters (HPC or FEMC) and hadronic calorimeters (HCAL) are clustered according to the spatial resolution of the given calorimeter to form bigger deposits which are likely to come from single particle showers. Then a matching between reconstructed charged particle tracks and the calorimeter showers is performed. The deposits not associated to any charged particle track are assumed to originate from a neutral particle cascade. Together with all reconstructed charged particle tracks they contribute to the total visible energy E_{vis} and to the computation of the hemisphere masses $M_{vis}^i (i \colon \Lambda_b$,oppo). For the reconstruction of hemisphere masses the formula $M^i = M_{vis}^i \frac{\sqrt{s}}{2E_{vis}}$ was found to be the best approximation. The correction accounts for both detector effects and for the missing neutrino.

The resolution of the neutrino energy reconstruction ($E_\nu^{rec} - E_\nu^{gen}$) obtained from the simulation is shown in Fig. 4. The two distributions correspond to contributions from purely hadronic Λ_c decays and semileptonic Λ_c decays. In the latter case there is an additional neutrino from the Λ_c decay escaping from the apparatus. The distributions for the hadronic Λ_c decays and semileptonic Λ_c decays were fitted with Gaussian functions

$\langle$E$\rangle$ (GeV)	data	simulation
muons, $P_{b-TAG} < 0.01$ $p > 3.0$ GeV$/c$, $p_T > 1.0$ GeV$/c$		
$\langle$E$\rangle_\mu$	10.30±0.07	10.38±0.07
$\langle$E$\rangle_{miss}$	8.89±0.11	8.90±0.11
$y = \langle$E$\rangle_\mu / \langle$E$\rangle_{miss}$	1.159±0.018	1.166±0.018
$\langle$E$\rangle^{oppo}$	41.39±0.12	41.03±0.12
electrons, $P_{b-TAG} < 0.01$ $p > 3.0$ GeV$/c$, $p_T > 1.0$ GeV$/c$		
$\langle$E$\rangle_e$	10.14±0.07	10.07±0.07
$\langle$E$\rangle_{miss}$	8.45±0.11	8.36±0.11
$y = \langle$E$\rangle_e / \langle$E$\rangle_{miss}$	1.200±0.018	1.205±0.018
$\langle$E$\rangle^{oppo}$	41.77±0.13	41.64±0.13

Table 3: Hemisphere energy in GeV reconstructed in the inclusive semileptonic events without requiring a Λ^0. For calculation of $\langle$E$\rangle^{oppo}$ the opposite hemispheres containing identified leptons with $p > 3.0$ GeV$/c$ have been excluded.

yielding widths of 4.2 GeV and 4.5 GeV, respectively. Moreover, the E_ν residuals for hadronic Λ_c decays are centered on zero while the semileptonic Λ_c decay subsample shows a large offset of ≈ 3.5 GeV equal to the average energy of the neutrino from the Λ_c decay. The analysis presented here did not distinguish between hadronic and semileptonic Λ_c decays in the real data. The two contributions were considered together and the $\frac{BR(\Lambda_c \to l\nu\Lambda^0 X)}{BR(\Lambda_c \to \Lambda^0 X)}$ found in the simulation was assumed. The uncertainty on this ratio was taken into account in the systematic error. The possibility of tagging double semileptonic decays by looking for another lepton (of the opposite sign) in the Λ_b hemisphere was investigated. It was found, however, to be ineffective due to the low average energy of the charged lepton from Λ_c decay. The decays giving most distortion of the missing energy spectrum have large neutrino energies and low lepton momenta where DELPHI has poor identification ability.

The stability of neutrino energy reconstruction versus Λ_b polarization was checked in the simulation as well. No systematic dependence was observed.

The data/simulation agreement on the missing energy was checked using different event samples within the hadronic event selection described at the beginning of section 4.3.

The total visible event energy comparison exhibits very good agreement between data and simulation. The average values agree to a few parts in a thousand. Such a comparison, however, is inclusive and moreover cannot reveal possible distortions from the hemisphere separation. Therefore, a final cross-check was done on an inclusive sample of b-hadron semileptonic decays.

The sample was selected requiring an identified energetic lepton ($p > 3.0$ GeV$/c$) with a high p_T ($p_T > 1.0$ GeV) contained in a b-tagged event ($P_{b-TAG} < 0.01$ corresponding to b purity of $\approx 85\%$). Since 90% of b's hadronize into mesons the inclusive sample should not retain any detectable polarization. Plots 5a–d show the comparison of the charged lepton and of the hemisphere missing energy, E_{miss}, spectra reconstructed in data and in the simulation. Plots in the left column correspond to the muon subsample and in

the right column to the electron subsample. Both charged lepton spectra and the E_{miss} spectra show good agreement between data and simulation. In addition, plots 5e and 5f show spectra of visible energy in the hemisphere opposite to the reconstructed lepton when this hemisphere did not have any identified leptons with $p > 3.0$ GeV/c. The detailed numerical results of the whole cross-check are summarised in Table 3. The table contains four quantities extracted for each sample:

    1. the average energy of the charged lepton (μ or e),

    2. the average missing energy in the lepton hemisphere obtained using the same algorithm as for the E_ν reconstruction,

    3. the ratio of the above two mean values which is the observable directly sensitive to polarization,

    4. the average energy of the opposite hemisphere; events that have identified leptons with $p > 3.0$ GeV/c in the opposite hemisphere are excluded.

Data/simulation discrepancies in both lepton and neutrino mean energies and in the resulting y value are within one standard deviation of their statistical uncertainty. Therefore, taking a conservative value of 2σ it can be assumed that the systematic error on $\langle E_\nu \rangle$ does not exceed 220 MeV.

5   The results

sample	background-free Λ_b simulation	$q\bar{q}$ MC 1992–1995	1992–1995 data
# of Λ_b candidates	2061±12	643±25	249±19
f_{bck}	0.032±0.004	0.33±0.02	0.41±0.04
$\langle E_l \rangle$ (GeV)	11.75±0.12	11.83±0.30	11.21±0.53
$\langle E_\nu \rangle$ (GeV)	7.46±0.15	7.34±0.37	5.86±0.65
y	1.58±0.04	1.61±0.10	$1.91^{+0.26}_{-0.22}$
R_y	1.0	1.02±0.06	$1.21^{+0.16}_{-0.14}$
P	0.0	$-0.05^{+0.16}_{-0.15}$	$-0.49^{+0.32}_{-0.30}$

Table 4: Analysis results obtained for the reference Λ_b simulation, the simulated unbiased $q\bar{q}$ events and the data. The quoted errors are statistical only.

The results obtained for the background-free reference Λ_b simulation, the simulated unbiased $q\bar{q}$ events and the data are summarised in Table 4. The R_y and polarization P for the background-free Λ_b simulation sample are by definition equal to one and zero respectively. The whole analysis applied to the simulation of the unbiased $q\bar{q}$ events gives a result which is compatible with zero and within their errors the observables are in good agreement with the ones obtained from the background-free reference simulation. This result additionally confirms the validity of assumptions about the background behaviour and its subtraction done in section 4.4. The last column of Table 4 gives relevant results extracted from the data. Fig. 6 shows the charged lepton and neutrino energy spectra for both *right-sign* and *wrong-sign* samples and for the Λ_b signal obtained from the subtraction. The statistical error on $\langle E_\nu \rangle$ is not much worse than on $\langle E_l \rangle$ because, although the resolution on an individual measurement of E_ν is poorer, the errors on the averages

are dominated by the width of the distributions. The result reads:

$$R_y = \frac{y^{data}}{y^{MC}} = 1.21\ ^{+0.16}_{-0.14}(stat.).$$
(7)

The polarization is extracted from this value of R_y using the calibration curve from Fig. 2c. Since the correlation between R_y and P_{Λ_b} is not linear the error on the latter becomes asymmetric. The Λ_b polarization is found to be:

$$P_{\Lambda_b} = -0.49\ ^{+0.32}_{-0.30}(stat.).$$
(8)

The systematic error estimation is described in the following section.

5.1 Systematic uncertainties

The individual contributions to the total systematic uncertainty, summarised in Table 5, are discussed below.

source	$\sigma(R_y)$
$BR(\Lambda_c^+ \to l\nu\Lambda^0 X)$	+0.060 −0.055
Λ_c polarization	±0.010
neutrino energy	+0.047 −0.044
background bias	±0.017
$\Lambda_b \to \tau\nu_\tau X$ and $\tau \to \nu_\tau l\nu_l$	+0.014
Λ_b fragmentation function	−0.018
MC reference	+0.020 −0.029
theory	±0.005
Total	**+0.082** **−0.080**

Table 5: Systematic error contributions.

As mentioned in section 4.5, there is a large offset in the reconstructed neutrino energy when the Λ_c decays semileptonically. Therefore, the result obviously depends on the semileptonic branching fraction of Λ_c, $R_{sl} = \frac{BR(\Lambda_c \to l\nu\Lambda^0 X)}{BR(\Lambda_c \to \Lambda^0 X)}$. Most of the uncertainty on this number is due to the poorly measured $BR(\Lambda_c \to \Lambda^0 X)$ which is estimated to be $(35 \pm 11)\%$ [24]. Taking the PDG value for the $BR(\Lambda_c \to l\nu\Lambda^0 X)$ leads to $R_{sl} = (9^{+5}_{-4})\%$. Assuming that the process $\Lambda_c \to l\nu\Lambda^0 X$ dominates the Λ_c semileptonic decays and the CLEO result for $BR(\Lambda_c \to e^+ X) = (3.4 \pm 0.4)\%$ [25], an estimate of the upper limit on $R_{sl} \leq (19^{+8}_{-5})\%$ is obtained. To account for this large uncertainty R_{sl} was allowed to vary by ±8% around the 14% assumed in the simulation. This variation corresponds to a systematic uncertainty on the measured missing energy of ±280 MeV leading to an error on R_y of $^{+0.060}_{-0.055}$.

The Λ_c polarization affects the average missing energy measurement in Λ_c semileptonic decays because the average energy of the neutrino escaping from Λ_c depends on the

polarization. Fortunately the dependence is not so strong in this process [11]. Therefore, the expected variation of the average reconstructed neutrino energy for unit change in Λ_c polarization does not exceed 50 MeV corresponding to $\sigma(R_y) = \pm 0.010$.

As discussed in section 4.5, a systematic discrepancy between data and simulation in the hemisphere energy estimation cannot fake the neutrino energy measurement by more than 220 MeV yielding $\sigma(R_y) = {}^{+0.047}_{-0.044}$.

Residual differences between the *wrong-sign* sample and the *right-sign* background can lead to a shift in the measured Λ_b polarization. The shift comes both from a different effective y reconstructed in the two samples and their unequal population faking the apparent f_{bck}. Possible sources of such biases were discussed in section 4.4. To extract the induced final systematic error they were added incoherently. The summed error on R_y does not exceed 0.017.

The contribution from $\Lambda_b \to \tau\nu_\tau X$ with the subsequent decay $\tau \to \nu_\tau l\nu_l$ gives rise to the extra *right-sign* $\Lambda^0 l$ correlations. This background source might lead to an error on the observed R_y of $+0.014$.

In principle the measurement should not be sensitive to the Λ_b fragmentation function. However, selection cuts, efficiency functions, etc. could introduce a certain limited dependence. The value of $\langle E_l \rangle$ observed in data is almost 2σ lower than expected under the assumption that the Λ_b fragmentation function is identical in data and in the simulation. The possible influence of the fragmentation on the polarization measurement was studied using the background-free Λ_b simulated events. In the subsequent event samples the generated Λ_b spectrum was varied in order to reproduce a large range of mean Λ_b energy. The linear fit to the y behaviour presented in Fig. 7 shows a very limited dependence of the reconstructed y on the Λ_b average energy. A variation of the mean Λ_b energy by as much as -25% (from 34.0 GeV to 25.5 GeV) corresponds to an error on the reconstructed R_y of -0.018.

Limited statistics of the simulated Λ_b calibration sample led to an uncertainty on R_y of ${}^{+0.020}_{-0.029}$.

The theoretical error arises mainly from the uncertainty on the value of m_c/m_b and is small. This uncertainty enters the analysis implicitly via the parameters of the Monte Carlo event generator. The value $m_c/m_b = 0.27$ was used. Variation in the large range between 0.20 and 0.36 corresponds to a systematic error on R_y smaller than 0.005 [26]. As mentioned already in the introduction, both QCD perturbative and non-perturbative corrections were neglected being tiny relative to other sources of systematic uncertainties.

All systematic error contributions were added in quadrature resulting in $\sigma(R_y) = {}^{+0.082}_{-0.080}$ corresponding to the total uncertainty on P_{Λ_b} of ± 0.17.

5.2   Consistency check using B mesons

B^0 mesons being scalar objects do not carry any polarization. The polarization measured on the B^0 sample should be consistent with zero. Therefore, an independent measurement of the B meson polarization can serve as a test of the consistency of the analysis.

Events of B^0 semileptonic decays via the process $B^0 \longrightarrow D^{*-}l^+\nu_l$ were selected [26]. The D^* mesons were reconstructed in the channel $D^{*-} \to \bar{D}^0 \pi^-_{soft}$ where $\bar{D}^0 \to K^+\pi^-$. Next, the D^* candidates were correlated with high p_T leptons found in the same hemisphere. The lepton selection was the same as the one described in section 4.1. A sample of 386 ± 9 $B^0 \longrightarrow D^{*-}l^+\nu_l$ signal candidates was collected.

The whole procedure to extract the polarization was identical with that used in the Λ_b analysis. The relevant polarization observables obtained from the data and the reference

sample	# of B^0 candidates	f_{bck}	$\langle E_l \rangle$ (GeV)	$\langle E_\nu \rangle$ (GeV)	y
MC $b\bar{b}$	2371±17	0.056±0.005	10.75±0.12	6.99±0.14	1.54±0.04
data	386±9	0.090±0.015	10.61±0.30	6.73±0.37	$1.58^{+0.11}_{-0.10}$

Table 6: Polarization observables for the $B^0 \longrightarrow D^{*-}l^+\nu_l$ decay measured in data and in the simulation of $b\bar{b}$ events.

simulation are summarised in Table 6. These yield the polarization:

$$P_B = -0.08 \pm 0.20 (stat.)^{+0.08}_{-0.07}(MC\ ref.), \tag{9}$$

where the second error is the systematic uncertainty coming only from the limited statistics of the Monte Carlo reference sample. The result is compatible with zero polarization in the B meson sector. Although the statistical significance of this result is limited it excludes the existence of a severe systematic discrepancy between data and MC in the missing energy estimation and proves the general correctness of the experimental procedure.

6 Conclusions

The Λ_b polarization has been measured using semileptonic decays selected from $\approx$ 3.5×10^6 hadronic Z^0 decays collected with the DELPHI detector between 1992 and 1995.

The Λ_b event selection is based on charge correlations in pairs of high p_T leptons and Λ^0 baryons found in the same event hemisphere. The final sample contains 249±19 Λ_b candidates observed as an excess of *right-sign* over *wrong-sign* Λl pairs.

The polarization is determined from the ratio of the average energies of charged leptons and neutrinos from Λ_b decays which is an experimental observable both highly sensitive to polarization and practically free from theoretical uncertainties.

The measured value of Λ_b polarization is:
$$P_{\Lambda_b} = -0.49\ ^{+0.32}_{-0.30}(\text{stat.})\ \pm 0.17(\text{syst.})$$
The result is in good agreement with those obtained by ALEPH [27] $(P_{\Lambda_b} = -0.23^{+0.24}_{-0.20}(stat.)^{+0.08}_{-0.07}(syst.))$ and OPAL [28] $(P_{\Lambda_b} = -0.56^{+0.20}_{-0.13}(stat.) \pm 0.09(syst.))$. Bearing in mind the SM prediction for b polarization of -0.94, within the model [6] (see Section 1) all three results favour the scenario where a substantial fraction of Λ_b's are produced in the decays of Σ_b and Σ_b^* states which live long enough to allow for a spin flip.

Acknowledgements

References

[1] B. Mele & G. Altarelli, Phys. Lett. **B299** (1993) 345.

[2] B. Mele, Mod. Phys. Lett. **A9** (1994) 1239.

[3] S. Jadach & Z. Was, Acta. Phys. Pol. **B15** (1984) 1151.

[4] J.G. Körner, A. Pilaftsis, and M. Tung, Z. Phys. **C63** (1994) 575.

[5] M. Neubert, "B Decays and the Heavy Quark Expansion"; CERN-TH-97-024, Feb. 1997; Second Edition of Heavy Flavours, edited by A.J. Buras and M. Lindner (World Scientific, Singapore) and the references therein.

[6] A.F. Falk & M.E. Peskin, Phys. Rev. **D49** (1994) 3320.

[7] J. Körner, Nucl. Phys. Proc. Suppl. **50**: 130-134, 1996.

[8] DELPHI Collab., P. Abreu et al., Zeit. Phys. **C67** (1995) 543.

[9] OPAL Collab., G. Alexander et al., Zeit. Phys. **C73** (1997) 569.

[10] Sjöstrand,T, Computer Physics Communications **82** (1994) 74.

[11] M. Jeżabek & J.H. Kühn, Nucl. Phys. **B320** (1989) 20.

[12] A. Czarnecki, M. Jeżabek and J.H. Kühn, Nucl. Phys. **B351** (1991) 70.

[13] A. Czarnecki et al., Phys. Rev. Lett. **73** (1994) 384.

[14] T. Mannel & G. Schuler, Phys. Lett. **B279** (1992) 194.

[15] J. Chay, H. Georgi, B. Grinstein, Phys. Lett. **B247** (1990) 399.

[16] A. Manohar & M. B. Wise, Phys. Rev. **D49** (1994) 1310.

[17] G. Bonvicini & L. Randall, Phys. Rev. Lett. **73** (1994) 392.

[18] C. Diaconu, M. Talby, J. Körner & D. Pirjol, Phys. Rev. **D53** (1996) 6186.

[19] DELPHI Collab., P. Aarnio et al., Nucl. Instrum. Methods **A303** (1991) 233.

[20] DELPHI Collab., P. Abreu et al., Nucl. Instrum. Methods **A378** (1996) 57.

[21] DELPHI Collab., P. Abreu et al., Zeit. Phys. **C73** (1996) 11.

[22] The LEP Experiments: ALEPH, DELPHI, L3 and OPAL, Nucl. Instrum. Meth. Phys. Res., **A378** (1996) 101.

[23] DELPHI Collab., P. Abreu et al., Z. Phys. **C68** (1995) 375.

[24] Particle Data Group, Review of particle physics, Eur. Phys. J. **C3** (1998) 1.

[25] CLEO Collab., Phys. Lett. **B323** (1994) 219.

[26] P. Brückman, "Study of the Λ_b Polarization in the DELPHI Experiment at LEP", Ph. D. dissertation, available from:
`http://wwwcn.cern.ch/~braize/thesis/bruckman/bruckman.ps.gz`

[27] ALEPH Collab., D. Buskulic et al., Phys. Lett. **B365** (1996) 437.

[28] OPAL Collab., G. Abbiendi et al., Phys. Lett. **B444** (1998) 539.
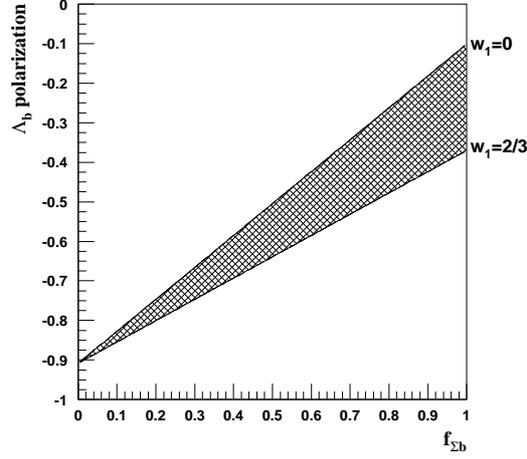
Figure 1: Theoretical prediction for the effective Λ_b polarization as a function of the fraction of Λ_b's produced indirectly through Σ_b and Σ_b^* states (f_{Σ_b}). The prediction holds only if Σ_b and Σ_b^* are distinct and narrow resonances.
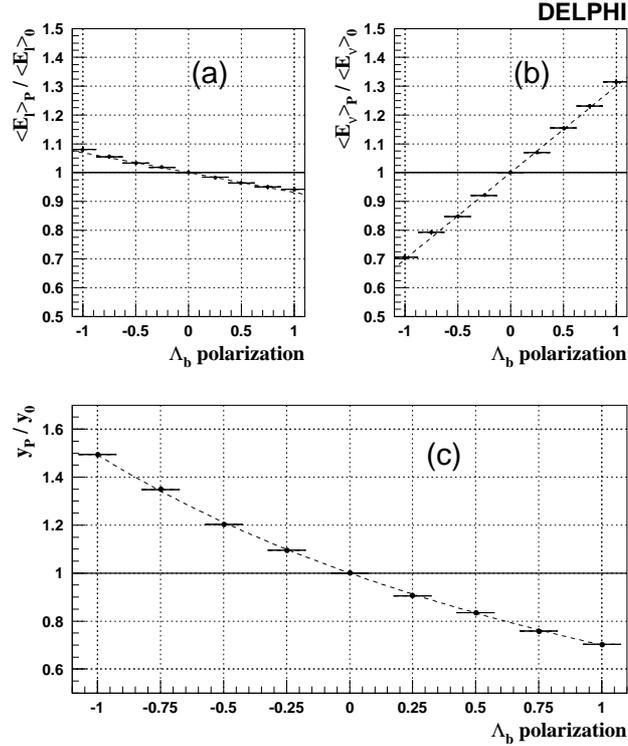
Figure 2: Dependence of the polarization observables on the Λ_b polarization as reconstructed in the simulation after the whole analysis procedure. The quantities are normalised to the unpolarized case. (a) charged lepton energy $\langle E_l \rangle / \langle E_l \rangle_{P=0}$; (b) neutrino energy $\langle E_\nu \rangle / \langle E_\nu \rangle_{P=0}$; (c) y variable $y/y_{P=0}$. The dashed lines are fits to the simulation points as described in the text. The strong dependence on polarization of the neutrino mean energy is a direct consequence of equation (2). The residual sensitivity of the charged lepton comes from the four-momentum conservation in the $l\nu\Lambda_c$ system. It is therefore diluted by the three-body decay kinematics.
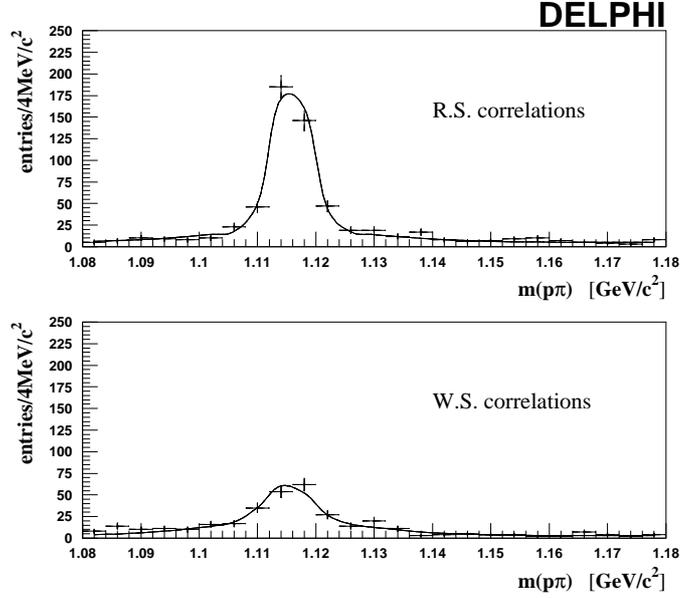
Figure 3: (pπ) mass distributions for Λ^0 candidates correlated with an identified high p$_T$ lepton in 1992–1995 data after the b-tagging selection described in the text. The excess of *right-sign* over *wrong-sign* events is attributed to the b baryon signal. The curves are the result of the double-Gaussian fits.
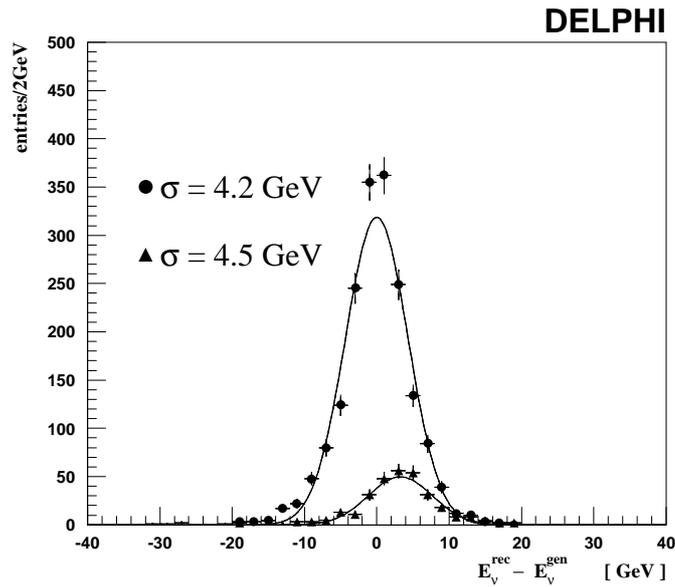
Figure 4: E_ν resolution obtained from the simulation of $\Lambda_b \to l\nu\Lambda^0 X$ events. Points show the contribution from hadronic Λ_c decays and triangles the contribution from semileptonic Λ_c decays. The curves result from the Gaussian fits.

DELPHI
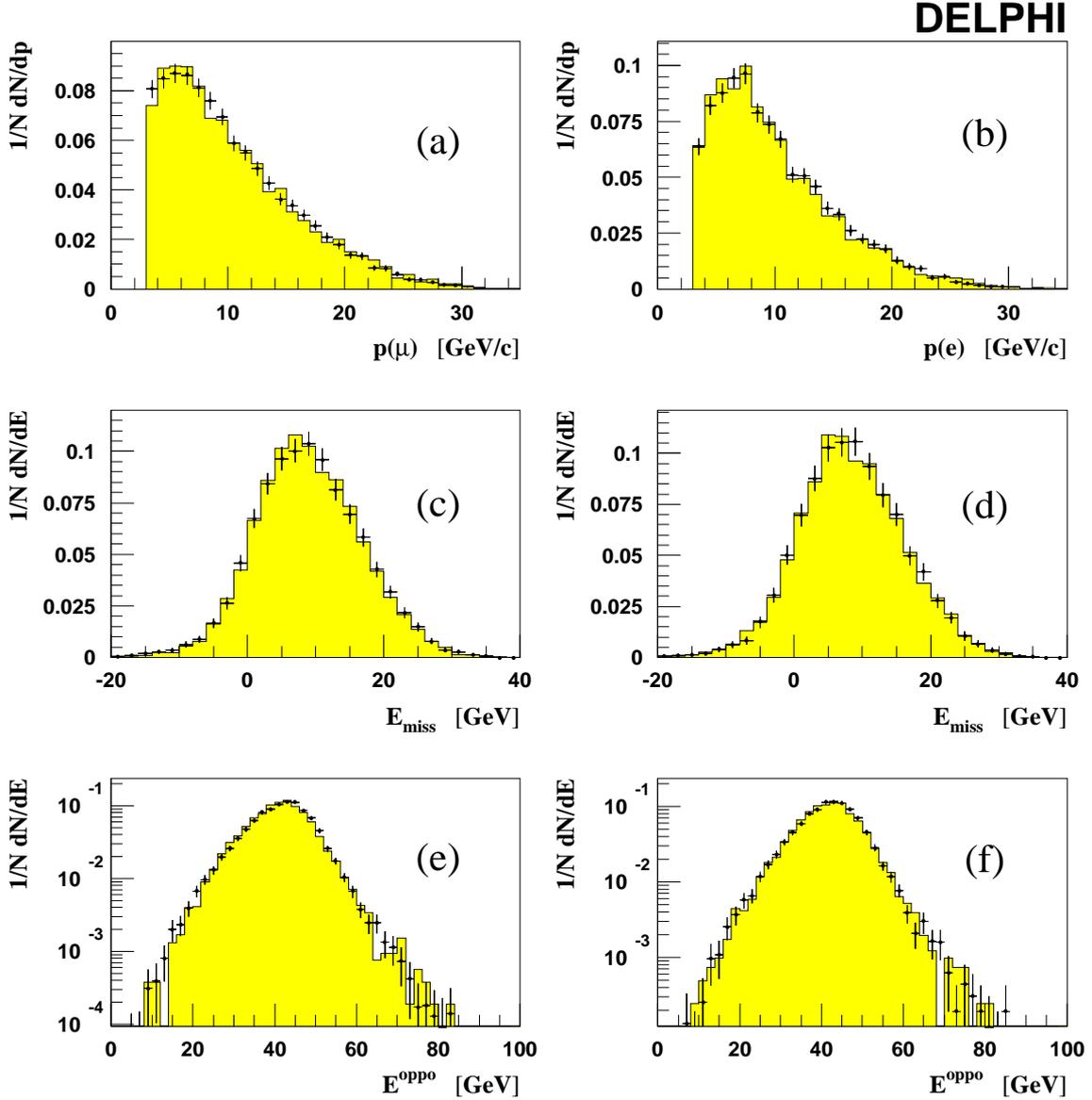
Figure 5: Comparison of different reconstructed energy spectra in the data (points with error bars) and in the simulation (shaded histogram). The global event selections were applied (see section 4.3). All histograms are normalized to the unit area. (a) momentum spectrum of identified muons with $p > 3.0$ GeV/c and $p_T > 1.0$ GeV/c in b-tagged events ($P_{btag} < 0.01$); (b) momentum spectrum of identified electrons with $p > 3.0$ GeV/c and $p_T > 1.0$ GeV/c in b-tagged events ($P_{btag} < 0.01$); (c) missing energy in the muon hemisphere (same sample as a); (d) missing energy in the electron hemisphere (same sample as b); (e) visible energy in the hemisphere opposite to the muon (same sample as a) but excluding events with an identified lepton with $p > 3.0$ GeV/c in this hemisphere; (f) visible energy in the hemisphere opposite to the electron (same sample as b) but excluding events with an identified lepton with $p > 3.0$ GeV/c in this hemisphere.
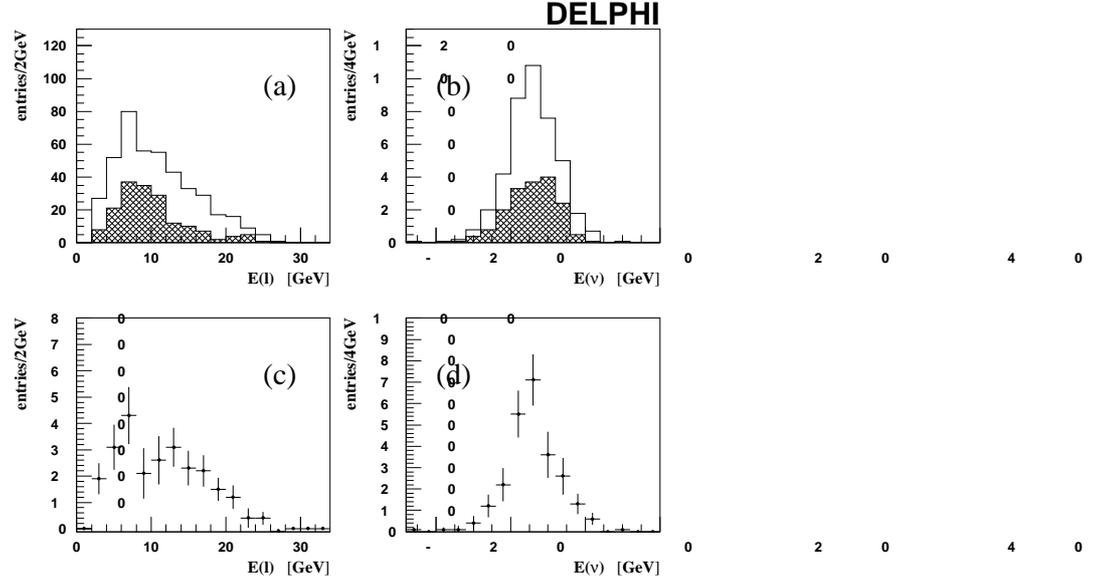
Figure 6: Lepton reconstructed energy spectra for the final $\Lambda^0 l$ sample found in data. Plots (a) and (c) show the charged lepton energy while plots (b) and (d) give corresponding distributions for the neutrino. The upper plots show distributions for *right-sign* (blank histogram) and *wrong-sign* (hatched histogram) $\Lambda^0 l$ pairs. The lower plots show the corresponding background subtracted spectra for the Λ_b signal (*right-sign* − *wrong-sign*).
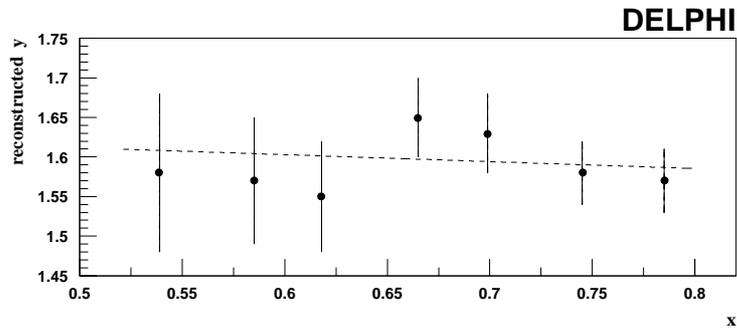
Figure 7: Dependence of the reconstructed y on the Λ_b fragmentation function in the background-free simulation. The plot shows corresponding reconstructed y values as a function of mean $x = \langle E_{\Lambda_b}/E_{beam} \rangle$. The dashed line represents the best linear fit to the points.